Electronic Supplementary Material

Floret-like Fe-N_x nanoparticle-embedded porous carbon superstructures from a Fe-covalent triazine polymer boosting oxygen electroreduction

Yong Zheng (✉)[1,4], Mingjin Li[1], Yongye Wang[1], Niu Huang[1,4], Wei Liu[1,4], Shan Chen[2], Xuepeng Ni[2], Kunming Li[2], Siwei Xiong[3], Yi Shen[5], Siliang Liu[6], Baolong Zhou[7], Niaz Ali Khan (✉)[8], Liqun Ye (✉)[1,4], Chao Zhang (✉)[2], Tianxi Liu[2]

1 College of Materials and Chemical Engineering, Key Laboratory of Inorganic Nonmetallic Crystalline and Energy Conversion Materials, China Three Gorges University, Yichang 443002, China

2 State Key Laboratory for Modification of Chemical Fibers and Polymer Materials, College of Materials Science and Engineering, Donghua University, Shanghai 201620, China

3 College of Materials Science and Engineering, Hubei Key Laboratory for New Textile Materials and Applications, Wuhan Textile University, Wuhan 430200, China

4 Hubei Three Gorges Laboratory, Yichang 443007, China

5 College of Environment, Zhejiang University of Technology, Hangzhou 310032, China

6 College of Light-Textile Engineering and Art, Anhui Agricultural University, Hefei 230036, China

7 School of Pharmacy, Weifang Medical University, Weifang 261053, China

8 Key Laboratory of Textile Fiber and Products (Wuhan Textile University), Ministry of Education, Wuhan 430200, China

E-mails: zhengyong@ctgu.edu.cn (Zheng Y); niaz2mn@hotmail.com (Khan N A); lqye@ctgu.edu.cn (Ye L); czhang@dhu.edu.cn (Zhang C)

Experimental methods

Materials

Cyanuric chloride (99%), piperazine (99%) and triethylamine (99.5%), iron (III) chloride (98%) were obtained from Aladdin Reagent Co, Ltd, China. Acetonitrile (AR, ≥ 99.0%), triethylamine (AR, ≥ 99.0%), acetone (AR, ≥ 99.0%), ethanol (99.5%), H_2SO_4 (AR, 95.0 ~ 98.0%) and zinc acetate dihydrate (AR, ≥ 99.0%) were purchased from Sinopharm Chemical Reagent Co, Ltd, China. Potassium hydroxide (KOH, GR, ≥ 90%) and nafion solution (5 wt%) were purchased from Sigma-Aldrich Co. Ltd. 20 wt% commercial Pt/C catalyst was purchased from Alfa Aesar chemical Co, Ltd, China. All these chemicals were used as received without further purification unless specified. Deionized water was produced by a laboratory water maker at 25 °C (18.2 $M\Omega \cdot cm^{-1}$ resistivity) and used throughout the experiments.

Characterizations

The solid-state ^{13}C nuclear magnetic resonance spectrum was confirmed on an AvanceIII400MHz instrument (Germany) with tetramethylsilane (TMS) as an internal standard. Fourier transform infrared spectrometer (FT-IR) spectra were measured utilizing a Perkin-Elmer Instrument. The X-ray photoelectron spectroscopy (XPS) was recorded on a Karatos Axis ULTRA spectrometer. The nitrogen adsorption and desorption isotherms were conducted at the liquid nitrogen (77 K) with a QUADRASORB SI automated surface area and pore size analyzer device (Quantachrome Corporation, USA), the specific surface area (SSA) of CTPS and resultant catalysts were received from the adsorption curves based on the Brunauer-Emmett-Teller (BET) equation and the calculation of pore-size distribution of samples were received, which were based on nonlocal density functional theory (DFT) equilibrium model. Before measurements, all the samples were outgassed at 120 °C in vacuum for 24 h. Raman spectra were carried out on a LabRAM ARAMIS system with a wavelength 633 nm laser. Powder X-ray diffraction (XRD) patterns of samples were received at an X-ray diffractometer on a Bruker D8 Advance. TGA was performed on TG 209 F1 from room temperature to 1000 °C in N_2 atmosphere with a heating rate of 10 °C min^{-1}. The

surface morphologies of the metal-coordinated polymer precursors and corresponding carbon catalysts were observed by field-emissions scanning electron microscopy (JEOL JSM-7500F) at an accelerating voltage of 5.0 kV. Transmission electron microscopy (TEM) was conducted through Talos F200S.

Electrochemical measurements

The ORR electrocatalytic activities of the catalysts were performed with CHI 660D electrochemical workstation in a standard three-electrode system using a graphite rod as the counter electrode, and the 5 mm diameter rotating disk electrode (RDE, Gamry Instruments, Inc.) loaded with catalysts as the working electrode. The catalyst ink was prepared by dispersing 5 mg of the catalysts into 350 μL of ethanol and 95 μL of Nafion solution (5 wt%). After sonication for 30 min, 5 μL catalyst ink was deposited onto the RDE (~290 μg cm^{-2} mass loading) and dried at room temperature naturally. For comparison, commercial Pt/C catalysts were used as a reference under same condition.

Rotating disk electrode (RDE) test: The ORR activities of catalysts were evaluated by cyclic voltammetry (CV) and linear sweep voltammetry (LSV) at the rotation rate of 800, 1200, 1600, 2000 and 2400 rpm, respectively, with O_2-saturated 0.1 M KOH solution as the electrolyte. All the potentials are transformed into a reference hydrogen electrode (RHE) using the following equations:

$$\mathrm{E\,(vs.\,RHE)} = \mathrm{E}\left(\mathrm{vs.}\frac{\mathrm{Ag}}{\mathrm{AgCl}}\right) + 0.197 + 0.059 \times \mathrm{pH}$$

The polarization curves were carried out in 0.1 M O_2-saturated KOH electrolyte with a potential range from -0.2 V to 1.2 V (vs. RHE) at a rotation speed of 1600 rpm. Before the RDE test, the electrodes were scanned for 100 CV cycles with a scan rate of 100 mV s^{-1} in O_2-saturated 0.1 M KOH to activate the catalyst. The electron transfer number (n) was calculated by linear fitting using the Koutecky-Levich (K-L) equation:

$$\frac{1}{j} = \frac{1}{B\omega^{1/2}} + \frac{1}{j_K}$$

$$B = 0.62nFC_0(D_0)^{2/3}v^{-1/6}$$

where j is the measured current density, F is the Faraday constant (F = 96485 C cm^{-1}), C_0 is the bulk concentration of O_2 (C_0 = 1.2*10^{-3} M), D_0 is the diffusion coefficient of oxygen (D_0

= $1.9*10^{-5}$ cm s^{-1}) in a 0.1 M KOH solution, *v* is the kinetic viscosity of the electrolyte (0.01 cm^2 s^{-1}), and *k* is the electron transfer rate constant. The value of *B* can be obtained from the slope of the K-L equation, and ω is the rotation rate. Thus, when B is known, the electron transfer number (n) can be calculated from the equation.

Rotating ring-disk electrode (RRDE) test: The catalytic performance of the catalyst towards ORR was performed via cyclic voltammetry (CV) at a scan rate of 50 mV s^{-1} and linear sweep voltammetry (LSV) at a scan rate of 5 mV s^{-1} on a rotating ring-disk electrode (RRDE), and ring electrode was also scanned. The yield of hydrogen peroxide and electron transfer number (n) were obtained from the equations as follows:

H_2O_2 (%) = 200*Ir/N/(I_d+Ir/N)

n = 4*I_d/(I_d+Ir/N)

in which I_d and I_r represent the disk and ring currents, and N is corresponding to the ring collection efficiency, which is provided as 0.37 by manufacture.

Zn-air battery measurements

The conventional Zn-air batteries were fabricated using a self-made acrylic resin cell and the measurements were conducted under ambient conditions. A hydrophobic carbon paper was provided as the current collector. A polished zinc plate (0.20 mm thickness) and 6.0 M KOH solution containing 0.2 M zinc acetate are served as the anode and electrolyte, respectively. The cathode was prepared with loading Fe/N@CNF-800 or commercial Pt/C catalysts on the 1 × 1 cm carbon cloth (~1.0 mg cm^{-2}).

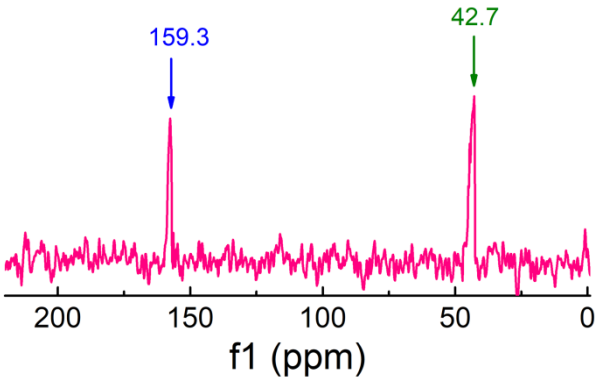

Fig. S1. Solid-state ^{13}C NMR spectrum of CTP.

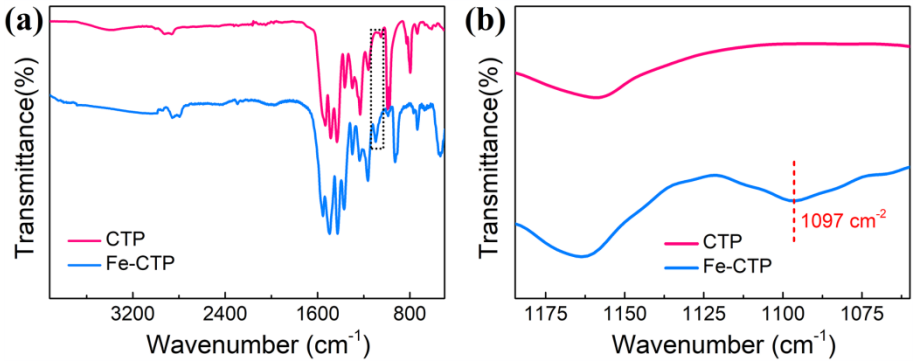

Fig. S2. FT-IR spectrum of Fe-CTP and CTP.

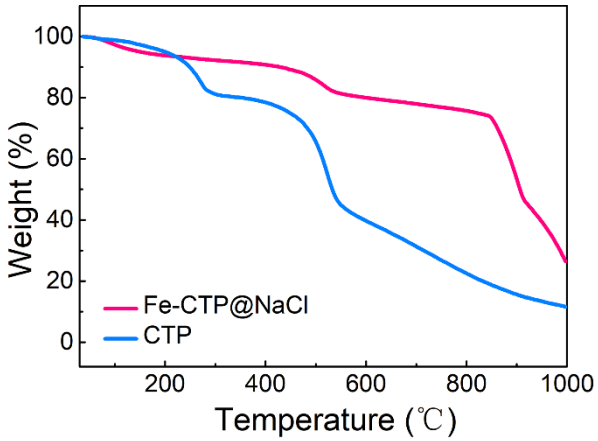

Fig. S3. TGA curves of the Fe-CTP@NaCl and CTP.

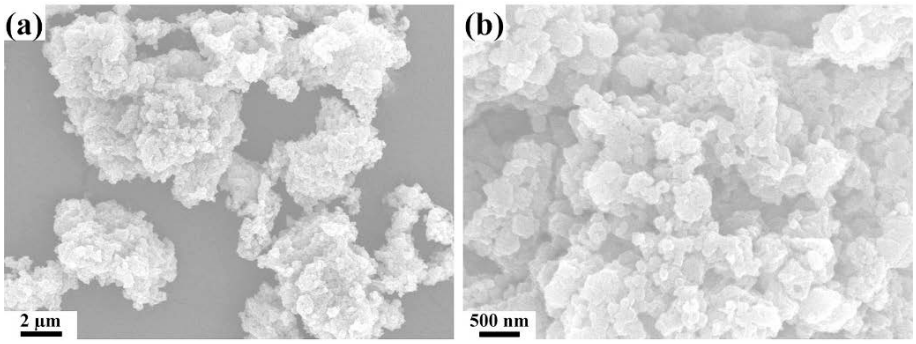

Fig. S4. SEM images of Fe-CTP at low and high magnifications, respectively.

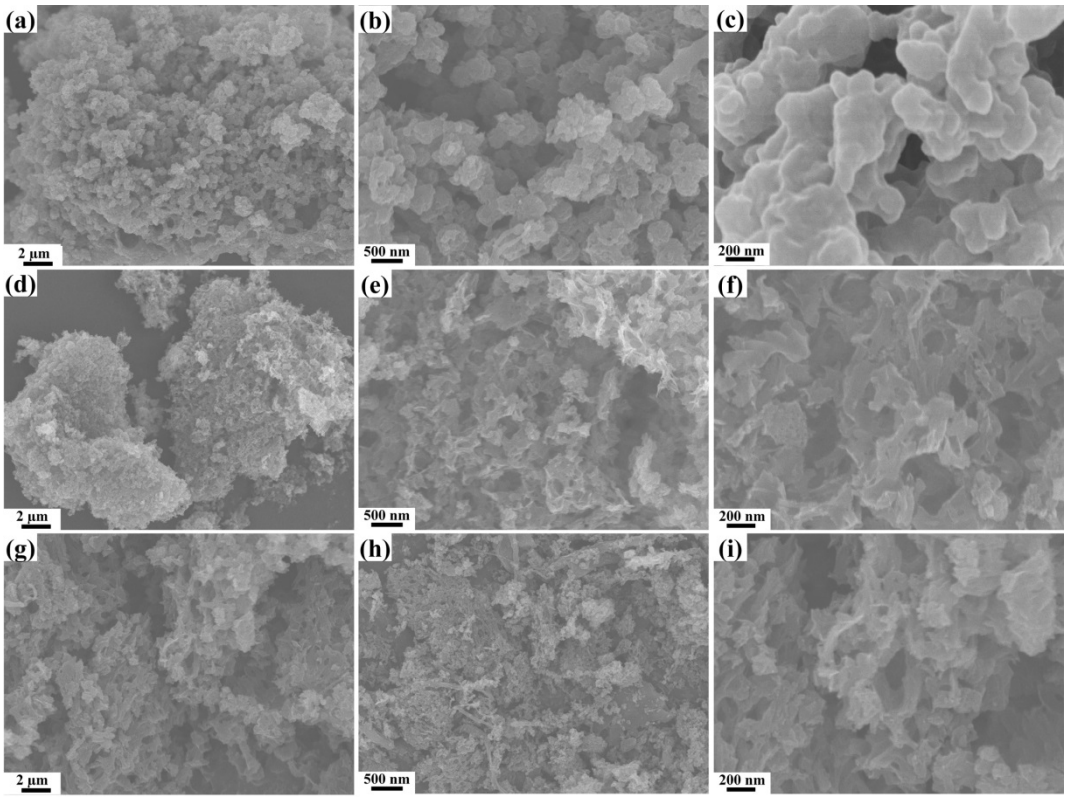

Fig. S5. SEM images of (a-c) Fe/N@CNF-700, (d-f) Fe/N@CNF-800, (g-i) Fe/N@CNF-900 at low and high magnifications, respectively.

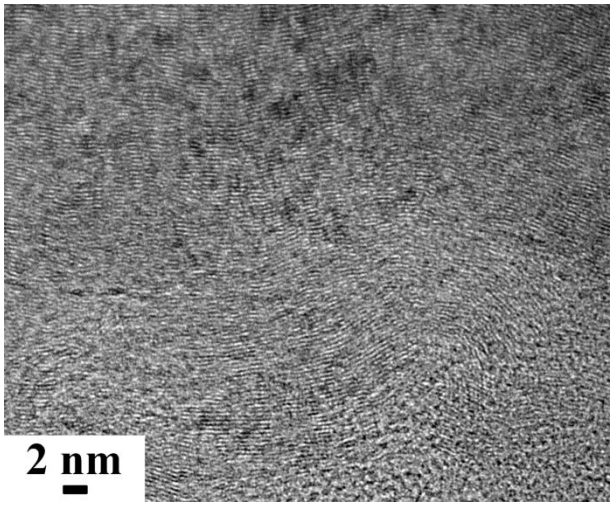

Fig. S6. HRTEM image of Fe/N@CNF-800.

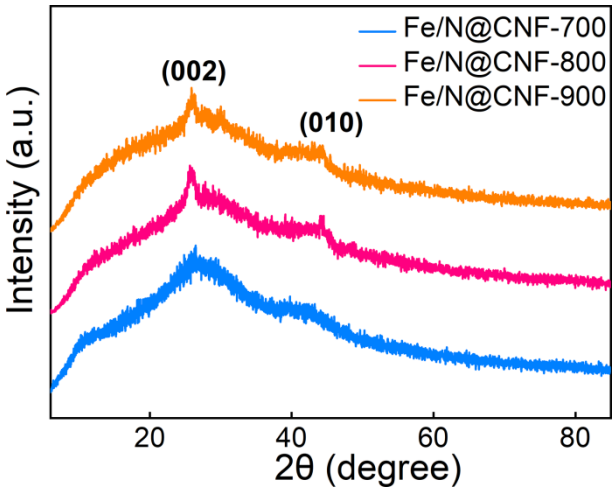

Fig. S7. XRD patterns of the Fe/N@CNFs.

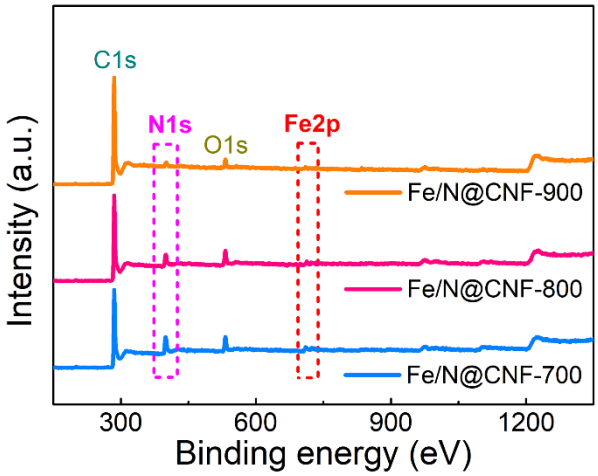

Fig. S8. XPS survey of Fe/N@CNF-700, Fe/N@CNF-800 and Fe/N@CNF-900 catalysts.

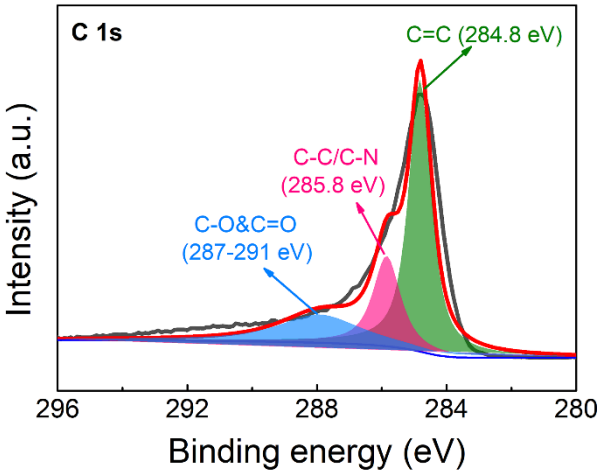

Fig. S9. High-resolution C 1s XPS spectra of Fe/N@CNF-800.

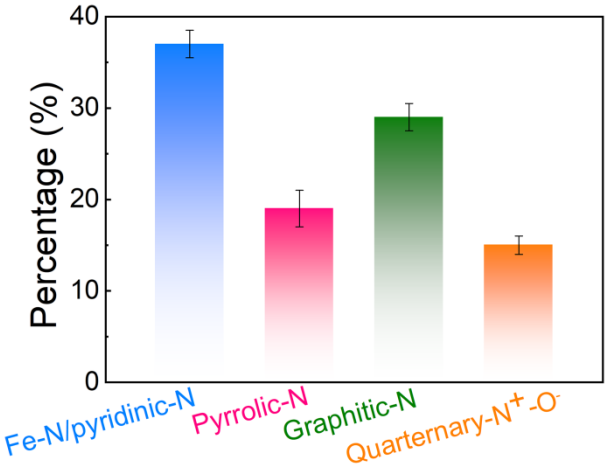

Fig. S10. The proportion of different doped-N types of Fe/N@CNF-800 catalyst.

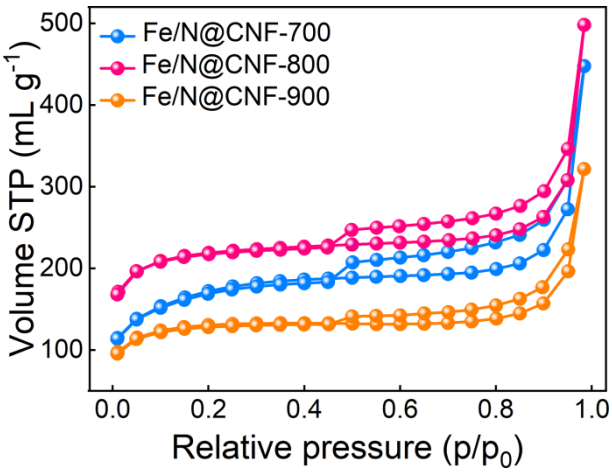

Fig. S11. Nitrogen adsorption/desorption isotherm of Fe/N@CNFs.

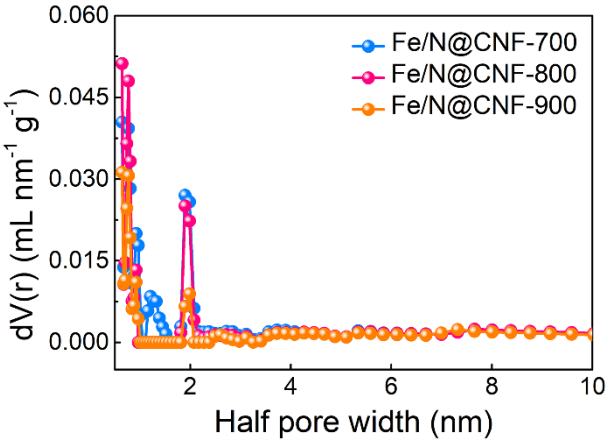

Fig. S12. The pore size distribution of the Fe/N@CNFs.

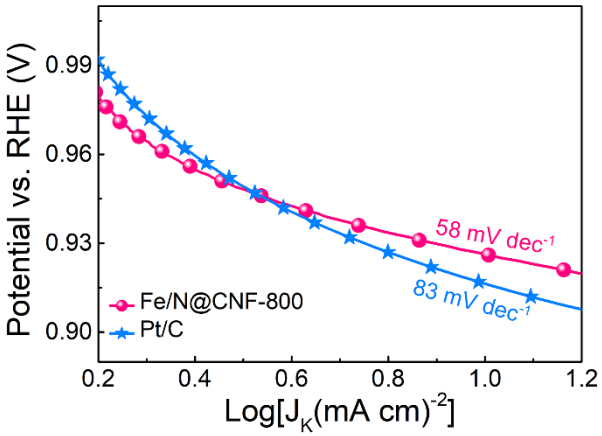

Fig. S13. Tafel curves of the different samples from corresponding ORR LSV curves.

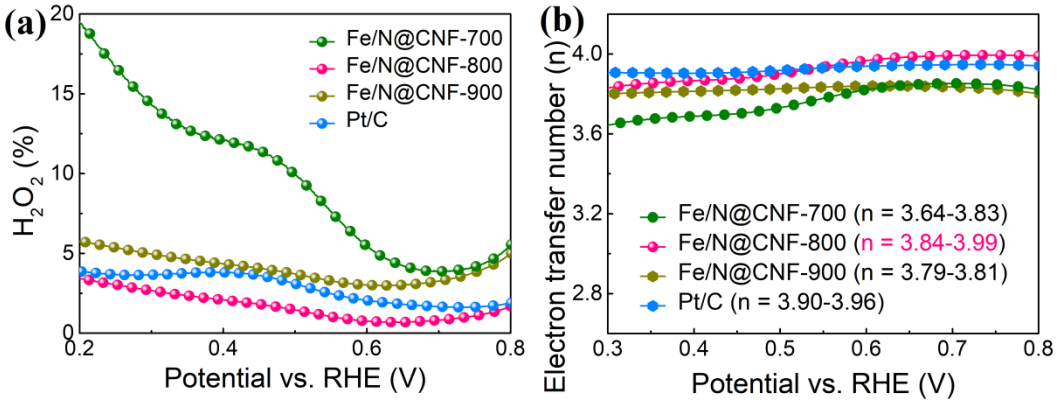

Fig. S14. (a) H_2O_2 yields and (b) calculated electron-transfer numbers of the FeN@CNF-800 derived from RRDE polarization curves in 0.1 M O_2-saturated KOH solution, 1600 rpm.

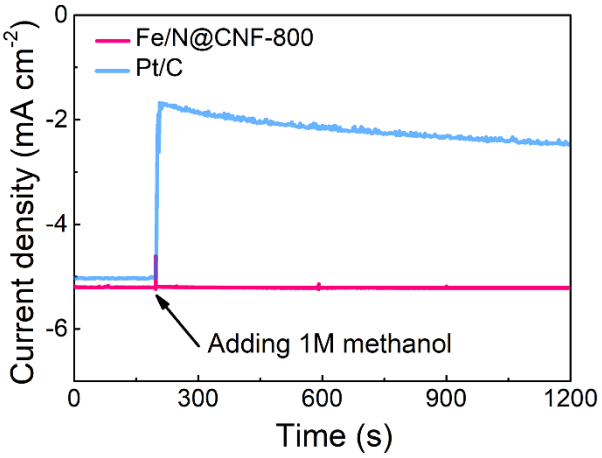

Fig. S15. (a) Chronoamperometric responses of Fe/N@CNF-800 and Pt/C catalysts upon addition of 1 M methanol, respectively.

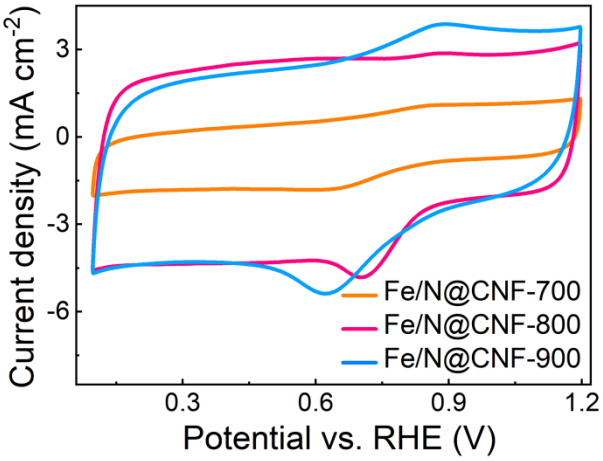

Fig. S16. CV curves of the Fe/N@CNFs in 0.1 M H_2SO_4 at scan rate 50 mV s^{-1}.

Table S1. Elemental compositions of Fe/N@CNFs determined by XPS results.

samples	C [at%]	N [at%]	Fe [at%]
Fe/N@CNF-700	77.24	14.54	1.21
Fe/N@CNF-800	**85.17**	**4.84**	**0.99**
Fe/N@CNF-900	91.03	4.11	0.51

Table S2. Comparison of our Fe/N@CNF-800 catalyst with some reported Fe-based ORR catalysts in 0.1 M KOH electrolyte.

catalysts	E_{onset} (V vs.RHE)	$E_{1/2}$ (V vs.RHE)	J_L (mA cm^{-2})	Ref.
Fe_3C-FeN/NC-2	0.95	0.82	5.02	[1]
Fe_3C/Fe_2O_3@N-CNTs	0.97	0.88	6.01	[2]
Fe-Zn-SA/NC	0.93	0.85	4.83	[3]
FeCo-NPs/NC	0.91	0.82	5.15	[4]
Fe-N/C-800	1.00	0.84	5.19	[5]
Ag-CoFe@NC-700	0.96	0.83	5.31	[6]
Fe-SASC	1.00	0.87	5.62	[7]
Co_3Fe_7/N, Mn-PC	0.98	0.87	5.87	[8]
Fe-NC/rOCNT	0.98	0.87	5.76	[9]
Timb-Fe_5-C	0.99	0.89	5.36	[10]
$Fe_{Fe\text{-}O\text{-}Fe}$-UP/CA	1.08	0.93	5.71	[11]

FeNC-NW	1.02	0.92	6.01	[12]
meso-Fe-N-C	0.92	0.85	5.68	[13]
Ni_3Fe-GA_1	0.93	0.80	4.52	[14]
Fe_{20}@N/HCSs	0.95	0.85	5.75	[15]
Co_3Fe_7@Fe_2N/rGO	0.95	0.79	5.41	[16]
MPC@PhFe	0.99	0.86	5.33	[17]
Fe/N@CNF-800	**1.02**	**0.89**	**5.15**	**this work**

Table S3. Comparison of some recently reported Fe-based ORR catalysts in acid condition.

Catalyst	ORR E_{onset} (V vs.RHE)	ORR $E_{1/2}$ (V vs.RHE)	J_L (mA cm^{-2})	Electrolyte	Ref.
Fe-Zn-SA/NC	0.87	0.78	4.72	0.1 M $HClO_4$	[3]
HSAC/Fe-3	0.94	0.81	4.53	0.5 M H_2SO_4	[18]
FeNC-NW	0.90	0.82	5.51	0.1 M $HClO_4$	[12]
HP-FeN_4	0.95	0.80	5.78	0.1 M $HClO_4$	[19]
FeN_4/HOPC-c-1000	0.90	0.78	4.52	0.5 M H_2SO_4	[20]
Fe-N-C/FeN	0.89	0.78	8.81	0.1 M $HClO_4$	[21]
FeNC-BP	0.84	0.69	5.54	0.1 M H_2SO_4	[22]
Co-Fe-S@NSRPC	0.86	0.80	5.01	0.5 M H_2SO_4	[23]
NGM-800	0.86	0.78	4.24	0.1 M $HClO_4$	[24]
Fe/N@CNF-800	**0.92**	**0.78**	**4.48**	**0.5 M H_2SO_4**	**This work**

Table S4. Comparison of the performance of Zn-air batteries with our Fe/N@CNF-800 catalyst and Fe-based catalysts.

air catalysts	open-circuit voltage [V]	power density [mW cm^{-2}]	Ref.
SA-Fe/NC	-	91	[25]
Si-Fe/S/N-RH_3	1.53	86	[26]
A-Fe-NC	1.45	132	[27]
$Fe_{0.5}Ni_{0.5}$@N	1.48	85	[28]
CoFe-Co@PNC	1.46	153	[29]
$Co_{0.7}Fe_{0.3}$@NC	1.45	86	[30]
Fe-N-C/N-OMC	1.55	113	[31]
CoFeP@C	-	144	[32]
FeS/Fe_3C@NS	1.46	91	[33]
SA-Fe-Nx-MPC	1.53	130	[34]
Ni_3FeN	1.55	-	[35]
Co/CoO@FeNC	1.42	133	[36]

Fe/Co-Nx-C	1.42	152	[37]
FeNSC800	1.52	60	[38]
HCSC-IV-H	1.43	105	[39]
FeCo-NPC	1.49	93	[40]
Fe/N@CNF-800	**1.51**	**164**	**This work**

Supplementary References

[1] F. Zhou, P. Yu, F. Sun, G. Zhang, X. Liu, L. Wang, The cooperation of Fe_3C nanoparticles with isolated single iron atoms to boost the oxygen reduction reaction for Zn–air batteries, J. Mater. Chem. A 9 (2021) 6831-6840.

[2] B. Zhang, T. Li, L. Huang, Y. Ren, D. Sun, H. Pang, J. Yang, L. Xu, Y. Tang, In situ immobilization of $Fe/Fe_3C/Fe_2O_3$ hollow hetero-nanoparticles onto nitrogen-doped carbon nanotubes towards high-efficiency electrocatalytic oxygen reduction, Nanoscale 13 (2021) 5400-5409

[3] J. Xu, S. Lai, D. Qi, M. Hu, X. Peng, Y. Liu, W. Liu, G. Hu, H. Xu, F. Li, C. Li, J. He, L. Zhuo, J. Sun, Y. Qiu, S. Zhang, J. Luo, X. Liu, Atomic Fe-Zn dual-metal sites for high-efficiency pH-universal oxygen reduction catalysis, Nano Res. 14 (2021) 1374-1381.

[4] D. Xie, D. Yu, Y. Hao, S. Han, G. Li, X. Wu, F. Hu, L. Li, H.-Y. Chen, Y.-F. Liao, S. Peng, Dual-Active Sites Engineering of N-Doped Hollow Carbon Nanocubes Confining Bimetal Alloys as Bifunctional Oxygen Electrocatalysts for Flexible Metal–Air Batteries, Small 17 (2021) 2007239.

[5] X.-T. Wu, L.-J. Peng, K. Xiao, N. Li, Z.-Q. Liu, Rational design and synthesis of hollow Fe–N/C electrocatalysts for enhanced oxygen reduction reaction, Chem. Commun. 57 (2021) 5258-5261.

[6] Y. Wang, H. Yuan, F. Liu, T. Hu, A triphasic nanocomposite with a synergetic interfacial structure as a trifunctional catalyst toward electrochemical oxygen and hydrogen reactions, J. Mater. Chem. A 9 (2021) 7114-7121.

[7] Y. Wang, Q. Li, L.-c. Zhang, Y. Wu, H. Chen, T. Li, M. Xu, S.-J. Bao, A gel-limiting strategy for large-scale fabrication of Fe–N–C single-atom ORR catalysts, J. Mater. Chem. A 9 (2021) 7137-7142.

[8] R.-M. Sun, Y.-Q. Yao, A.-J. Wang, K.-M. Fang, L. Zhang, J.-J. Feng, One-step pyrolysis synthesis of nitrogen, manganese-codoped porous carbon encapsulated cobalt-iron nanoparticles with superior catalytic activity for oxygen reduction reaction, J. Colloid and Interf. Sci. 592 (2021) 405-415.

[9] J. Sheng, S. Zhu, G. Jia, X. Liu, Y. Li, Carbon nanotube supported bifunctional electrocatalysts containing iron-nitrogen-carbon active sites for zinc-air batteries, Nano Res. (2021).

[10] X. Lin, P. Peng, J. Guo, L. Xie, Y. Liu, Z. Xiang, A new steric tetra-imidazole for facile synthesis of high loading atomically dispersed FeN_4 electrocatalysts, Nano Energy 80 (2021) 105533.

[11] J. Shi, X. Shu, C. Xiang, H. Li, Y. Li, W. Du, P. An, H. Tian, J. Zhang, H. Xia, Fe ultra-small particles anchored on carbon aerogels to enhance the oxygen reduction reaction in Zn-air batteries, J. Mater. Chem. A (2021).

[12] X. Zhu, B. Hu, C. Wang, X. An, J. He, X. Wang, Y. Zhao, Self-assembly induced metal ionic-polymer derived Fe-Nx/C nanowire as oxygen reduction reaction electrocatalyst, J. Catal. 391 (2020) 1-10.

[13] Y. Zhou, Y. Yu, D. Ma, A.C. Foucher, L. Xiong, J. Zhang, E.A. Stach, Q. Yue, Y. Kang, Atomic Fe Dispersed Hierarchical Mesoporous Fe–N–C Nanostructures for an Efficient Oxygen Reduction Reaction, ACS Catal. (2020) 74-81.

[14] Z. Wang, X. Liao, Z. Lin, F. Huang, Y. Jiang, K.A. Owusu, L. Xu, Z. Liu, J. Li, Y. Zhao, Y.-B. Cheng, L. Mai, 3D Nitrogen-Doped Graphene Encapsulated Metallic Nickel–Iron Alloy Nanoparticles for Efficient

Bifunctional Oxygen Electrocatalysis, Chemistry – A European Journal 26 (2020) 4044-4051.
[15] B. Wang, Y. Ye, L. Xu, Y. Quan, W. Wei, W. Zhu, H. Li, J. Xia, Space-Confined Yolk-Shell Construction of Fe_3O_4 Nanoparticles Inside N-Doped Hollow Mesoporous Carbon Spheres as Bifunctional Electrocatalysts for Long-Term Rechargeable Zinc–Air Batteries, Adv. Funct. Mater. 30 (2020) 2005834.
[16] D. Liang, H. Zhang, X. Ma, S. Liu, J. Mao, H. Fang, J. Yu, Z. Guo, T. Huang, MOFs-derived core-shell Co_3Fe_7@Fe_2N nanopaticles supported on rGO as high-performance bifunctional electrocatalyst for oxygen reduction and oxygen evolution reactions, Mater. Today Energy 17 (2020) 100433.
[17] M. Li, L. Fan, Z. Xiao, L. Zhang, Z. Wang, Z. Kang, H. Guo, F. Dai, X. Lu, D. Sun, Micelles of Mesoporous Silica with Inserted Iron Complexes as a Platform for Constructing Efficient Electrocatalysts for Oxygen Reduction, ACS Appl. Mater. Interfaces (2020).
[18] J. Guo, B. Li, Q. Zhang, Q. Liu, Z. Wang, Y. Zhao, J. Shui, Z. Xiang, Highly Accessible Atomically Dispersed Fe-Nx Sites Electrocatalyst for Proton-Exchange Membrane Fuel Cell, Adv. Sci. n/a (2021) 2002249.
[19] N. Zhang, T. Zhou, M. Chen, H. Feng, R. Yuan, C.a. Zhong, W. Yan, Y. Tian, X. Wu, W. Chu, C. Wu, Y. Xie, High-purity pyrrole-type FeN_4 sites as a superior oxygen reduction electrocatalyst, Energy Environ. Sci. 13 (2020) 111-118.
[20] M. Qiao, Y. Wang, Q. Wang, G. Hu, X. Mamat, S. Zhang, S. Wang, Hierarchically Ordered Porous Carbon with Atomically Dispersed FeN_4 for Ultraefficient Oxygen Reduction Reaction in Proton-Exchange Membrane Fuel Cells, Angew. Chem., Int. Ed. 59 (2020) 2688-2694.
[21] X. Luo, X. Wei, H. Wang, W. Gu, T. Kaneko, Y. Yoshida, X. Zhao, C. Zhu, Secondary-Atom-Doping Enables Robust Fe–N–C Single-Atom Catalysts with Enhanced Oxygen Reduction Reaction, Nano-Micro Lett. 12 (2020) 163.
[22] D. Jain, V. Gustin, D. Basu, S. Gunduz, D.J. Deka, A.C. Co, U.S. Ozkan, Phosphate tolerance of nitrogen-coordinated-iron-carbon (FeNC) catalysts for oxygen reduction reaction: A size-related hindrance effect, J. Catal. 390 (2020) 150-160.
[23] W. Fang, Z. Bai, X. Yu, W. Zhang, M. Wu, Pollen-derived porous carbon decorated with cobalt/iron sulfide hybrids as cathode catalysts for flexible all-solid-state rechargeable Zn–air batteries, Nanoscale 12 (2020) 11746-11758.
[24] W. Xia, J. Tang, J. Li, S. Zhang, K.C.-W. Wu, J. He, Y. Yamauchi, Defect-Rich Graphene Nanomesh Produced by Thermal Exfoliation of Metal–Organic Frameworks for the Oxygen Reduction Reaction, Angew. Chem., Int. Ed. 58 (2019) 13354-13359.
[25] L. Yang, D. Cheng, H. Xu, X. Zeng, X. Wan, J. Shui, Z. Xiang, D. Cao, Unveiling the high-activity origin of single-atom iron catalysts for oxygen reduction reaction, Proceedings of the National Academy of Sciences 115 (2018) 6626-6631.
[26] F. Wang, Q. Li, Z. Xiao, B. Jiang, J. Ren, Z. Jin, X. Tang, Y. Chen, X. Li, Conversion of rice husk biomass into electrocatalyst for oxygen reduction reaction in Zn-air battery: Effect of self-doped Si on performance, J. Colloid and Interf. Sci. 606 (2022) 1014-1023.
[27] N. Shang, C. Wang, X. Zhang, S. Gao, S. Zhang, T. Meng, J. Wang, H. Wang, C. Du, T. Shen, J. Huang, Y. Qiao, Q. Wu, Y. Gao, Atomically dispersed iron on nitrogen-decorated carbon for high-performance oxygen reduction and zinc-air batteries, Chem. Eng. J. 426 (2021) 127345.
[28] P. Liu, D. Gao, W. Xiao, L. Ma, K. Sun, P. Xi, D. Xue, J. Wang, Self-Powered Water-Splitting Devices by Core–Shell NiFe@N-Graphite-Based Zn–Air Batteries, Adv. Funct. Mater. 28 (2018) 1706928.
[29] Z. Lei, Y. Tan, Z. Zhang, W. Wu, N. Cheng, R. Chen, S. Mu, X. Sun, Defects enriched hollow porous Co-N-doped carbons embedded with ultrafine CoFe/Co nanoparticles as bifunctional oxygen electrocatalyst for rechargeable flexible solid zinc-air batteries, Nano Res. 14 (2021) 868-878.

[30] L. Long, H. Liu, J. Jia, Y. Zhang, S. Dong, $Co_{0.7}Fe_{0.3}$ NPs confined in yolk–shell N-doped carbon: engineering multi-beaded fibers as an efficient bifunctional electrocatalyst for Zn–air batteries, Nanoscale (2021).
[31] J. Han, H. Bao, J.-Q. Wang, L. Zheng, S. Sun, Z.L. Wang, C. Sun, 3D N-doped ordered mesoporous carbon supported single-atom Fe-N-C catalysts with superior performance for oxygen reduction reaction and zinc-air battery, Appl. Catal. B Environ. 280 (2021) 119411.
[32] L. Gao, S. Chang, Z. Zhang, High-Quality CoFeP Nanocrystal/N, P Dual-Doped Carbon Composite as a Novel Bifunctional Electrocatalyst for Rechargeable Zn–Air Battery, ACS Appl. Mater. Interfaces (2021).
[33] Y.-W. Li, W.-J. Zhang, J. Li, H.-Y. Ma, H.-M. Du, D.-C. Li, S.-N. Wang, J.-S. Zhao, J.-M. Dou, L. Xu, Fe-MOF-Derived Efficient ORR/OER Bifunctional Electrocatalyst for Rechargeable Zinc–Air Batteries, ACS Appl. Mater. Interfaces 12 (2020) 44710-44719.
[34] X. Fu, G. Jiang, G. Wen, R. Gao, S. Li, M. Li, J. Zhu, Y. Zheng, Z. Li, Y. Hu, L. Yang, Z. Bai, A. Yu, Z. Chen, Densely accessible Fe-Nx active sites decorated mesoporous-carbon-spheres for oxygen reduction towards high performance aluminum-air flow batteries, Appl. Catal. B Environ. (2021) 120176.
[35] G. Fu, Z. Cui, Y. Chen, L. Xu, Y. Tang, J.B. Goodenough, Hierarchically mesoporous nickel-iron nitride as a cost-efficient and highly durable electrocatalyst for Zn-air battery, Nano Energy 39 (2017) 77-85.
[36] Y. Chen, C. Gong, Z. Shi, D. Chen, X. Chen, Q. Zhang, B. Pang, J. Feng, L. Yu, L. Dong, Molten-salt-assisted synthesis of onion-like Co/CoO@FeNC materials with boosting reversible oxygen electrocatalysis for rechargeable Zn-air battery, J. Colloid and Interf. Sci. 596 (2021) 206-214.
[37] S. Yuan, L.-L. Cui, Z. Dou, X. Ge, X. He, W. Zhang, T. Asefa, Nonprecious Bimetallic Sites Coordinated on N-Doped Carbons with Efficient and Durable Catalytic Activity for Oxygen Reduction, Small 16 (2020) 2000742.
[38] Y. She, J. Liu, H. Wang, L. Li, J. Zhou, M.K.H. Leung, Bubble-like Fe-encapsulated N,S-codoped carbon nanofibers as efficient bifunctional oxygen electrocatalysts for robust Zn-air batteries, Nano Res. 13 (2020) 2175-2182.
[39] W. Yang, Y. Zhang, X. Liu, L. Chen, M. Liu, J. Jia, Polymerization-dissolution strategy to prepare Fe, N, S tri-doped carbon nanostructures for Zn-Air batteries, Carbon 147 (2019) 83-89.
[40] B. Guo, Q. Ju, R. Ma, Z. Li, Q. Liu, F. Ai, M. Yang, S. Kaskel, J. Luo, T. Zhang, J. Wang, Mechanochemical synthesis of multi-site electrocatalysts as bifunctional zinc–air battery electrodes, J. Mater. Chem. A 7 (2019) 19355-19363.